Demonstration of harmonic interaction in an undulator up to the 15th order

D. Xiang, E. Hemsing, M. Dunning, C. Hast, T. O. Raubenheimer, and S. Weathersby
SLAC National Accelerator Laboratory, Menlo Park, California, 94025, USA

F. Fu
Department of Physics, Shanghai Jiao Tong University, Shanghai, 200240, China
(Received 12 July 2013; published 12 November 2013)

We report on experimental studies on the harmonic interaction between an optical laser and a relativistic electron beam in an undulator up to the 15th order. In this experiment, a significant energy modulation is imprinted on the beam longitudinal phase space through the electron-laser interaction when the laser frequency is the 3rd, 5th, 7th, 9th or 15th harmonic of the fundamental resonant frequency of the undulator. The experimental results are in good agreement with theory, and indicate that high harmonic interactions in undulators with large K values and small phase errors can be quite efficient. The results confirm the basic physics of harmonic interaction with a goal toward ushering forward the development of many high harmonic based applications in free-electron lasers.

DOI: 10.1103/PhysRevSTAB.16.110701 PACS numbers: 41.60.Cr, 41.75.Ht

I. INTRODUCTION

When a relativistic electron beam goes through an undulator, monochromatic radiation at discrete frequencies is generated. The wavelength of the on-axis radiation from a planar undulator is

$$\lambda_n = \frac{1 + K^2/2}{2n\gamma^2}\lambda_u, \tag{1}$$

where γ is the relativistic factor of the beam, n is an odd number, and $K = 0.934\lambda_u[\mathrm{cm}]B[\mathrm{T}]$ is the dimensionless undulator strength that is related to both the undulator period λ_u and undulator peak field B. In synchrotron light sources, radiation produced in short undulators, both at fundamental and high harmonic frequencies (see [1] for example), is used in a wide range of scientific research. In free-electron lasers (FELs), the radiation interacts resonantly with the electron beam in longer undulators, leading to an instability that amplifies the radiation exponentially while also packing electrons into microbunches. These density-modulated electrons radiate in phase and emit coherent radiation with orders of magnitude higher power than the spontaneous radiation in synchrotrons. This makes FELs unique in providing high-power, short-wavelength radiation [2,3].

Recently, there has been growing interest in utilizing the harmonic interaction in FELs to reach shorter wavelengths, to reduce beam energies, or to improve the overall FEL performance. For example, an FEL that operates in harmonic lasing mode ($n > 1$) provides access to shorter wavelengths for fixed beam and undulator parameters [4–9]. The harmonic emission efficiency can be strongly enhanced if the fundamental wavelength is suppressed and the radiation output is dominated by one of the high harmonics [10–12]. Alternatively, for a given radiation wavelength, harmonic lasing may be driven by electron beams with lower energy to reduce the size and cost of FEL facilities. The harmonic interaction has the further benefit that the slippage between beam and radiation is increased by the harmonic number, which provides an *in situ* method for communicating phase information over larger portions of the electron beam in order to enhance the temporal coherence of the output light [13,14]. For example, in a purified self-amplified spontaneous emission (pSASE) FEL, a few undulator sections placed in the middle stage of exponential growth (called the slippage-boosted sections) with harmonics tuned to the FEL fundamental are predicted to reduce the FEL bandwidth [13]. By interacting at the 7th harmonics, amplification of the radiation is maintained in the slippage-boosted sections and enables, for example, enhancement of the spectral brightness of a standard SASE FEL by a factor of 5 [13]. Even higher harmonics (e.g. $n > 7$) are envisioned to further reduce the FEL bandwidth by this method.

In addition to potential benefits for FELs, the harmonic interaction between an input laser and an electron beam in an undulator also allows one to lower the required beam energy for injection into an inverse FEL (IFEL) [15], promising further reductions in the size of such advanced accelerators. Furthermore, harmonic interactions may be used to create tighter microbunches for increasing the capture efficiency in IFELs [16,17] and for increasing the bunching at high harmonics for FEL seeding [18–20]. Laser driven harmonic interactions have been reported by several groups, with $n = 2$ in [21], $n = 3$ in [22], $n = 6$ in [23], and $n = 7$ in [24].

In this paper we report on observation and measurement of harmonic interactions up to $n = 15$, a regime where numerous undesirable effects (e.g. undulator phase errors [25]) start to play important roles in high harmonic applications. In this experiment, an electron beam energy was varied incrementally from 120 MeV down to 54 MeV to examine the 3rd through the 15th odd harmonics with an 800 nm laser in a $N_u = 10$ period planar undulator with $\lambda_u = 55$ mm and $K = 2.76$. From direct measurements of the induced electron beam energy modulation, our studies indicate that in realistic conditions harmonic coupling remains efficient to at least the 9th order, with the 15th harmonic still showing a considerable interaction. This suggests a promising path toward harmonic-based applications in modern FELs and IFELs.

II. HARMONIC INTERACTION AND EXPECTED UNDULATOR PERFORMANCE

When an electron beam goes through an undulator (a magnet array of alternating dipoles), the alternating magnetic field makes the electrons wiggle in the transverse direction, and a sustained energy exchange between the electrons and the light may be achieved when the resonant condition Eq. (1) is met. Strong harmonics can arise in planar undulators because the longitudinal velocity has an oscillatory component $v_z(z) = c(1 - \frac{1+K^2/2}{2\gamma^2}) - \frac{K^2 c}{4\gamma^2} \times \cos(4\pi z/\lambda_u)$ that generates spontaneous emission at harmonic frequencies of the fundamental, where c is the speed of light. The on-axis single electron emission spectrum from an ideal planar undulator is given by [26]

$$\frac{dN_p}{d\omega} = \frac{\alpha}{\pi^2 \omega}\left[\frac{n\gamma K J J_n}{1 + K^2/2}\right]^2 \frac{\sin^2[N_u \pi(\omega/\omega_1 - n)]}{(\omega/\omega_1 - n)^2}, \quad (2)$$

where N_p is the number of photons at the frequency ω, α is the fine structure constant, and $\omega_1 = 2\pi c/\lambda_1$ is the fundamental frequency. The coupling factor JJ_n characterizes the efficiency of interaction at the nth harmonic,

$$JJ_n = J_{(n-1)/2}\left(\frac{nK^2}{4 + 2K^2}\right) - J_{(n+1)/2}\left(\frac{nK^2}{4 + 2K^2}\right), \quad (3)$$

where J_i is the Bessel function of the ith order.

In ideal planar undulators with $N_u \gg 1$, the on-axis emission spectrum has sharp peaks at the odd harmonics, each with a relative bandwidth $1/nN_u$. In practice, however, several factors including undulator phase errors or the electron beam energy spread, emittance, and spot size can modify the output spectrum and affect the on-axis brightness. In terms of undulator phase errors, the reduction in brightness at high harmonics may be estimated by the quantity $R = \exp(-n^2\sigma_\phi^2)$, where σ_ϕ is the accumulated root mean square (rms) phase error in radians [25]. The phase error describes the difference between the phase in a real undulator with errors and that in an ideal undulator. It corresponds to the flight time variation due to the variation of the trajectory length that results in unwanted destructive interferences.

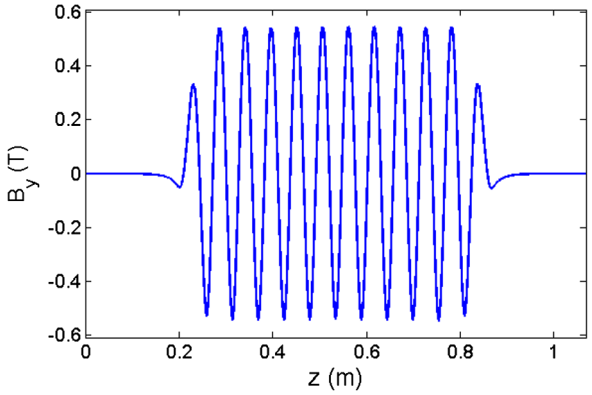

FIG. 1. Measured magnetic fields of the 10-period undulator U55 with $K = 2.76$ at various longitudinal positions.

To gauge the expected magnitude of this effect, we first examined the calculated emission spectrum of our $\lambda_u = 55$ mm, 10-period undulator called U55. Originally built by STI Optronics [27] for a proof-of-principle echo-enabled harmonic generation (EEHG) experiment [28,29], the U55 undulator has been recently retuned to $K = 2.76$ to allow seeding with a 2.4 μm laser. The measured on-axis magnetic field of U55 is shown in Fig. 1. Through careful shimming and optimization, the measured rms phase error of U55 is about 2 degrees, which by itself indicates good performance at high harmonics (e.g. $R = 0.76$ with $n = 15$ and $R = 0.33$ with $n = 30$). The phase error is determined from the measurement of the slippage in this undulator scaled with radiation wavelength. Figure 2 shows the on-axis photon flux of U55 calculated using the synchrotron radiation workshop code [30] and the measured magnetic field. Emission at high harmonics up to $n \approx 31$ is anticipated from the single electron simulations, while larger harmonics appear smeared out by the phase error. In contrast, much higher

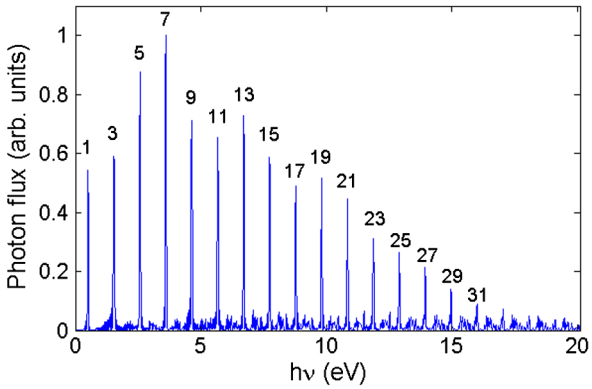

FIG. 2. Single electron on-axis photon flux from a 120 MeV electron. In the simulation the radiation is integrated over a 0.1 mm by 0.1 mm area at a distance 4 m downstream of the undulator.

harmonics can be seen in simulations of an ideal 10-period undulator with the same K value (not shown).

The calculated emission spectrum for the measured undulator field is illustrative because it establishes the expected limits on the harmonic coupling. There are many methods for studying high harmonics in an undulator. A conceptually straightforward technique is to measure the photon flux at various harmonics for fixed beam and undulator parameters, and compare the results with expectations [31]. However, this requires one to accurately measure the spectrum over a wide frequency range, extending in our case from the IR to the extreme ultraviolet. Alternately, the fact that the beam radiates in an undulator implies that the beam can exchange energy with a laser with the same wavelength as the spontaneous radiation when they copropagate through the undulator [32]. This is the basic physics behind the IFEL interaction, and it enables us to quantify the efficiency of harmonic interaction by varying beam energy and directly measuring the induced energy spread growth from harmonic electron-laser interaction with a laser having fixed wavelength.

The resonant interaction induces a sinusoidal energy modulation in the electron beam that can be measured in an energy spectrometer. Assuming a Gaussian profile for the laser beam with an rms transverse size σ_r, the peak energy modulation for an electron located at radius r from the beam-laser interaction may be calculated as [33]

$$\Delta\gamma_n(r) = \sqrt{\frac{P_L}{P_0}}\frac{KL_u}{\gamma\sigma_r}JJ_n \exp\left(-\frac{r^2}{4\sigma_r^2}\right), \tag{4}$$

where P_L is the peak laser power, $P_0 \approx 8.7$ GW, and L_u is the undulator length. From Eq. (4), a laser spot size that is comparable to the transverse electron beam dimension leads to a reduction in the induced energy modulation amplitude, which has to be taken into account experimentally.

As with the emission spectrum, the laser-induced energy change also scales with the factor JJ_n, which identifies the values of K required for efficient harmonic coupling. The coupling strengths at various orders for an ideal undulator are shown in Fig. 3. Clearly for $K < 1$, only a few of the lowest harmonics exchange energy efficiently, while for $K \gg 1$ the coupling strength at high harmonics remains considerably large and decays slowly with n. This confirms analytic expectations that the U55 value of $K \simeq 2.76$ alone (red triangles) is sufficient to provide efficient harmonic coupling up to $n = 30$ in the absence of phase errors and other effects described below.

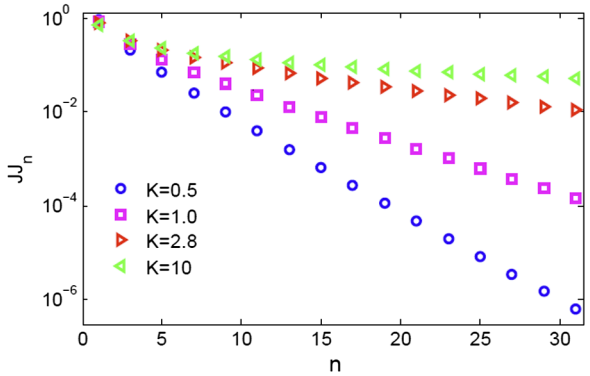

FIG. 3. Coupling strengths for various harmonic orders.

III. EXPERIMENTAL RESULTS

The experiment was carried out at SLAC's Next Linear Collider Test Accelerator (NLCTA) facility using the EEHG beam line. As shown in Fig. 4, the electron beam with ~20 pC charge is generated in a 1.6 cell S-band (2.856 GHz frequency) photocathode radio-frequency (rf) gun with a UV laser [~ 1 ps FWHM (full width at half maximum)] and further accelerated to a maximal energy of 120 MeV with X-band (11.424 GHz rf frequency) linac structures. In this experiment, a titanium-sapphire laser (~ 1 ps FWHM, ~300 μJ) with central wavelength at 800 nm is injected into U55 with a mirror in the upstream chicane. The sinusoidal energy modulation produced by the laser-electron interaction is measured with a high resolution energy spectrometer.

With quadrupole magnets (not shown) upstream of the energy spectrometer set to minimize the horizontal beta function at the yttrium aluminium garnet screen, the o ptimized beam energy distribution when the beam energy is 120 MeV is shown in Fig. 5(a). The distribution has a sharp edge on the right side (corresponding to the on-crest particles with the highest energy) and a short tail on the left (corresponding to the off-crest particles). From the sharp edge, the energy resolution in our measurement is estimated to be approximately 7 keV.

To make the laser interact with the electron beam, they need to overlap both spatially and temporally in the undulator. The spatial overlap is achieved by steering the laser beam with two remote-controlled mirrors to the same position as the electron beam on the optical transition radiation (OTR) screens (see Fig. 4) upstream and downstream of U55. The temporal overlap is achieved in two steps. First, the laser and undulator radiation generated by the electron beam is sent to a fast photodiode for determining the rough temporal offset of the laser beam and the electron beam; then a delay stage is used to finely adjust the relative timing until the growth of beam energy spread is observed at the screen downstream of the energy spectrometer. The energy spread growth is from the

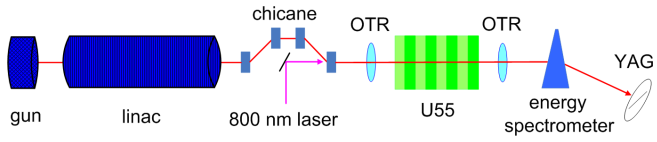

FIG. 4. Schematic layout of the harmonic interaction experiment at SLAC's NLCTA.

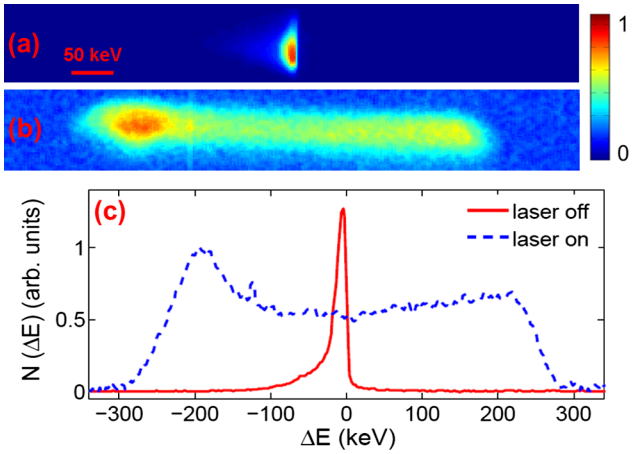

FIG. 5. Measured beam energy distributions with laser off (a) and laser on (b) at 120 MeV (corresponding to the 3rd harmonic interaction). The beam intensity in (a) is reduced by a factor of 10 to avoid saturation using the same scaling as (b). The projections of beam energy distributions in (a) and (b) are shown in (c).

3rd harmonic interaction between the 120 MeV beam and 800 nm laser (fundamental resonant wavelength of U55 is 2.4 μm).

The energy distribution of the 120 MeV beam with the laser on is shown in Fig. 5(b) where a double-horn shape is clearly seen. This shape can only be obtained when the transverse electron beam size [$\sigma_e \approx 100$ μm (rms)] is smaller than the laser spot size [$\sigma_r \approx 800$ μm (rms)], and when the electron bunch length (about 0.5 ps FWHM with velocity bunching in the gun [34]) is shorter than the laser pulse length such that the modulation amplitude is roughly uniform across the whole bunch [35]. The sinusoidal energy modulation, together with the rf curvature results in a double-horn shape in beam energy distribution, with the low-energy horn slightly larger than the high-energy horn. The FWHM of the projected energy distribution equals approximately twice the peak energy modulation which is found to be about 230 keV, in good agreement with that obtained with Eq. (4).

Following the observation of 3rd harmonic interaction, 5th, 7th, and 9th harmonic interactions are similarly studied by reducing electron beam energy to 93, 79, and 69 MeV, respectively. In this experiment, the magnetic fields of the chicane was accordingly reduced following the reduction of beam energy to keep the momentum compaction constant (constant path length in the chicane) such that the relative timing between the laser and electron beam is roughly maintained. After the energy spread growth from beam-laser interaction is seen, the beam energy and laser timing are finely adjusted to maximize the energy spread growth. The measured beam energy distribution for these higher harmonic interactions (not shown) have similar double-horn shapes as that observed in the thirrd harmonic interaction. The measured peak

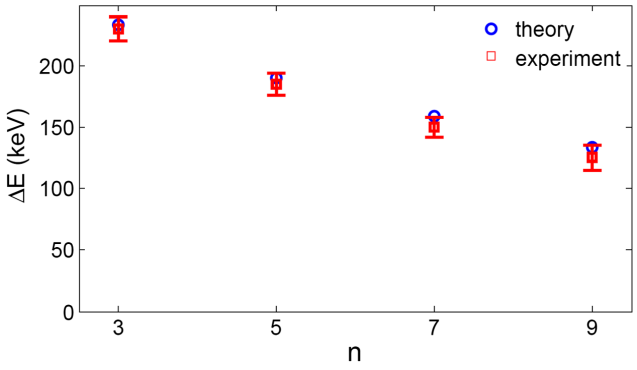

FIG. 6. Measured peak energy modulation amplitudes for harmonic interactions at various orders. The theoretical values are calculated assuming a perfect undulator with no phase error and a beam with exact on-resonance energy.

energy modulations for the 3rd, 5th, 7th, and 9th harmonic interactions are shown in Fig. 6 and they are in good agreement with the theoretical values calculated with Eq. (4) assuming an ideal undulator (note, $R = 0.91$ for $n = 9$, so the phase error effect may be neglected).

Finally, the beam energy was reduced to about 54 MeV which is on the edge of the accessible parameter space in our machine to test the 15th order harmonic interaction (fundamental resonant wavelength of U55 is 12 μm). Because the EEHG beam line is designed for a 120 MeV beam, the stability of power supply for the magnets at low currents is not as good as that at high currents, which leads to a less stable beam at low energy. Furthermore, OTR yield is lower at lower energy, which together with the relatively large beam size reduces the accuracy of the spatial overlap between the laser and electron beam in U55. Nevertheless, significant energy spread growth was still produced with the laser interacting with the beam through

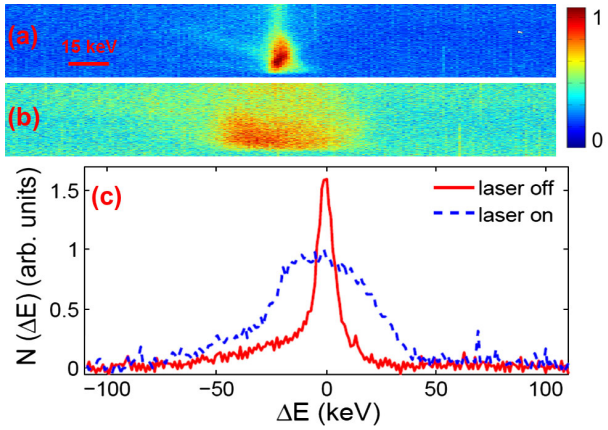

FIG. 7. Measured beam energy distributions with laser off (a) and laser on (b) at about 54 MeV (corresponding to the 15th harmonic interaction). The beam intensity in (a) is reduced by a factor of 2 to avoid saturation using the same scaling as (b). The projections of beam energy distributions in (a) and (b) are shown in (c).

the 15th order harmonic interaction (Fig. 7). Because the electron beam size in U55 was comparable to that of the laser, the beam energy distribution takes a Gaussian shape [Fig. 7(c)], similar to that produced in the so-called laser heater [35]. The energy spread is found to be about 23 keV and the peak energy modulation is estimated to be about 45 keV (see, for example, Eq. (1) in [35]).

The measured energy modulation amplitude for $n = 15$ is about a factor of 2 smaller than the theoretical value. Part of the deviation may be attributed to undulator phase errors. For instance, with a phase error of 2 degrees for U55, a 25% reduction in photon flux at $n = 15$ is estimated. This corresponds to about 13% reduction in radiation field and a similar degradation to laser energy modulation should be expected as well, because an electron's energy change can be calculated from the interference between the undualtor radiation field and laser field. Furthermore, the imperfect beam-laser spatial overlap and the relatively large orbit amplitude (about 0.23 mm) in the undulator at such a low energy may result in a smaller energy modulation amplitude too. We plan to have more systematic study at this ultrahigh harmonic regime in the future.

IV. SUMMARY AND DISCUSSIONS

In summary, we have presented experimental demonstration of high harmonic interaction up to the 15th order. We have shown that significant sinusoidal energy modulation can be produced trough electron-laser harmonic interactions when the laser frequency is the harmonic of the fundamental resonant frequency of the undulator. Our studies indicate that in general high harmonic interactions in undulators with large K values and small phase errors can be quite efficient. The results confirm the basic physics of harmonic interaction and paves the way for applying many high harmonic interaction-based techniques (e.g. harmonic lasing, pSASE, etc.) to enhance FEL performance.

ACKNOWLEDGMENTS

We thank X. Huang for useful discussions and Y. Levashov for undulator tuning and magnetic field measurements. This work was supported by the U.S. DOE Office of Basic Energy Sciences using the NLCTA facility which is partly supported by the U.S. DOE Office of High Energy Physics under Contract No. DE-AC02-76SF00515.

[1] E. Gluskin, J. Synchrotron Radiat. **5**, 189 (1998).
[2] Z. Huang and K.-J. Kim, Phys. Rev. ST Accel. Beams **10**, 034801 (2007).
[3] B. W. J. McNeil and N. R. Thompson, Nat. Photonics **4**, 814 (2010).
[4] W. B. Colson, Phys. Rev. A **24**, 639 (1981).
[5] S. Benson and J Madey, Phys. Rev. A **39**, 1579 (1989).
[6] R. Warren, L. Haynes, D. Feldman, W. Stein, and S. Gitomer, Nucl. Instrum. Methods Phys. Res., Sect. A **296**, 84 (1990).
[7] G. Neil, S. Benson, G. Biallas, J. Gubeli, K. Jordan, S. Myers, and M. Shinn, Phys. Rev. Lett. **87**, 084801 (2001).
[8] R. Hajima, R Nagai, N Nishimori, N Kikuzawa, and E. Minehara, Nucl. Instrum. Methods Phys. Res., Sect. A **475**, 43 (2001).
[9] S. Norihiro, O. Hiroshi, and Y. Kawakatsu, J. Phys. Soc. Jpn. **79**, 093501 (2010).
[10] B. W. J. McNeil, G. R. M. Robb, M. W. Poole, and N. R. Thompson, Phys. Rev. Lett. **96**, 084801 (2006).
[11] J. Dai, H. Deng, and Z. Dai, Phys. Rev. Lett. **108**, 034802 (2012).
[12] E. A Schneidmiller and M. V Yurkov, Phys. Rev. ST Accel. Beams **15**, 080702 (2012).
[13] D. Xiang, Y. Ding, Z. Huang, and H. Deng, Phys. Rev. ST Accel. Beams **16**, 010703 (2013).
[14] C. Feng, H. Deng, G. Wang, D. Wang, Z. Zhao, and D. Xiang, Phys. Rev. ST Accel. Beams **16**, 060705 (2013).
[15] R. Palmer, J. Appl. Phys. **43**, 3014 (1972).
[16] S. Pottorf and X. J. Wang, in *18th Advanced ICFA Beam Dynamics Workshop on Quantum Aspects of Beam Physics*, edited by P. Chen (World Scientific, Singapore, 2002), p. 232.
[17] J. P. Duris, P. Musumeci, and R. K. Li, Phys. Rev. ST Accel. Beams **15**, 061301 (2012).
[18] G. Stupakov and M. Zolotorev, in *Proceedings of the 33st International Free Electron Laser Conference (FEL 2011), Shanghai, China* (Shanghai Institute of Applied Physics, Shanghai, Chine, 2011), pp. 45–48.
[19] D. Ratner and A. Chao, in *Proceedings of the 33st International Free Electron Laser Conference (FEL 2011), Shanghai, China* (Shanghai Institute of Applied Physics, Shanghai, Chine, 2011), pp. 53–56.
[20] E. Hemsing and D. Xiang, Phys. Rev. ST Accel. Beams **16**, 010706 (2013).
[21] P. Musumeci, S. Ya. Tochitsky, S. Boucher, C. E. Clayton, A. Doyuran, R. J. England, C. Joshi, C. Pellegrini, J. E. Ralph, J. B. Rosenzweig, C. Sung, S. Tolmachev, G. Travish, A. A. Varfolomeev, A. A. Varfolomeev, Jr., T. Yarovoy, and R. B. Yoder, Phys. Rev. Lett. **94**, 154801 (2005).
[22] M. Dunning, E. Hemsing, C. Hast, T. O. Raubenheimer, S. Weathersby, D. Xiang, and F. Fu, Phys. Rev. Lett. **110**, 244801 (2013).
[23] C. M. S. Sears, E. Colby, B. M. Cowan, R. H. Siemann, J. E. Spenser, R. L. Byer, and T. Plettner, Phys. Rev. Lett. **95**, 194801 (2005).
[24] S. Ya. Tochitsky, O. B. Williams, P. Musumeci, C. Sung, D. J. Haberberger, A. M. Cook, J. B. Rosenzweig, and C. Joshi, Phys. Rev. ST Accel. Beams **12**, 050703 (2009).
[25] R. Walker, Phys. Rev. ST Accel. Beams **16**, 010704 (2013).
[26] A. Chao and M. Tigner, *Handbook of Acelerator Physics and Engineering*, 3rd printing (World Scientific, Singapore, 2006).
[27] STI Optronics, Inc. 'http://www.stioptronics.com/'.
[28] D. Xiang, E. Colby, M. Dunning, S. Gilevich, C. Hast, K. Jobe, D. McCormick, J. Nelson, T. O. Raubenheimer, K.

Soong, G. Stupakov, Z. Szalata, D. Walz, S. Weathersby, M. Woodley, and P.-L. Pernet, Phys. Rev. Lett. **105**, 114801 (2010).

[29] D. Xiang, E. Colby, M. Dunning, S. Gilevich, C. Hast, K. Jobe, D. McCormick, J. Nelson, T. O. Raubenheimer, K. Soong, G. Stupakov, Z. Szalata, D. Walz, S. Weathersby, and M. Woodley, Phys. Rev. Lett. **108**, 024802 (2012).

[30] O. Chubar and P. Elleaume, in *Proceedings of the 6th European Particle Accelerator Conference, Stockholm, 1998* (IOP, London, 1998), pp. 1177–1179.

[31] L. Giannessi, M. Artioli, M. Bellaveglia, F. Briquez, E. Chiadroni, A. Cianchi, M. E. Couprie, G. Dattoli, E. Di Palma, G. Di Pirro, M. Ferrario, D. Filippetto, F. Frassetto, G. Gatti, M. Labat, G. Marcus, A. Mostacci, A. Petralia, V. Petrillo, L. Poletto, M. Quattromini, J. V. Rau, J. Rosenzweig, E. Sabia, M. Serluca, I. Spassovsky, and V. Surrenti, Phys. Rev. Lett. **108**, 164801 (2012).

[32] R. B. Palmer, AIP Conf. Proc. **335**, 90 (1995).

[33] P. Musumeci, C. Pellegrini, and J. Rosenzweig, Phys. Rev. E **72**, 016501 (2005).

[34] X. J. Wang, X. Qiu, and I. Ben-Zvi, Phys. Rev. E **54**, R3121 (1996).

[35] Z. Huang, A. Brachmann, F.-J. Decker, Y. Ding, D. Dowell, P. Emma, J. Frisch, S. Gilevich, G. Hays, Ph. Hering, R. Iverson, H. Loos, A. Miahnahri, H.-D. Nuhn, D. Ratner, G. Stupakov, J. Turner, J. Welch, W. White, J. Wu, and D. Xiang, Phys. Rev. ST Accel. Beams **13**, 020703 (2010).